Mineralogical Magazine, May 2018, Vol. 82(S1), pp. S43–S59

Deposition conditions for the indium-bearing polymetallic quartz veins at Sarvlaxviken, south-eastern Finland

C. Broman[1], K. Sundblad[2,3,*], M. Valkama[2] and A. Villar[2]

[1] Department of Geological Sciences, Stockholm University, Stockholm, Sweden
[2] Department of Geography and Geology, University of Turku, Turku, Finland
[3] Institute of Earth Sciences, Saint Petersburg State University, Saint Petersburg, Russia

[*Received 10 January 2017; Accepted 16 April 2017; Associate Editor: Nigel Cook*]

ABSTRACT

Polymetallic quartz veins, with up to 1500 ppm indium, have been discovered recently in the Sarvlaxviken area within the 1.64 Ga anorogenic multiphase Wiborg rapakivi batholith and adjacent 1.90 Ga Svecofennian crust in SE Finland. Evidence from primary fluid inclusions in the Sarvlaxviken area provides new information on the hydrothermal transport and depositional processes of metals in anorogenic granites. Fluid inclusions with variable aqueous liquid and vapour proportions (5–90 vol.% vapour) occur in quartz, cassiterite and fluorite belonging to three generations of polymetallic quartz veins. Microthermometry indicates that the veins were deposited at temperatures that range from ~500°C down to <100°C and salinities from 0 to 16 eq. mass% NaCl. Fluid inclusion data show that the depositional conditions were similar regardless of vein generation. The interpreted depositional processes involve phase separation with a combination of condensation, cooling and boiling of an initially low-salinity (<3 eq. mass% NaCl) aqueous magmatic vapour phase enriched in CO_2-F-Cl-S and metals. Fluid inclusions with low salinities dominate, but higher salinities are recorded in metal-rich parts of the veins. The turbulent fluid flow, with complex geometry and temperature-salinity patterns, may explain why sulfide and/or oxide opaque minerals occur irregularly, and are locally the dominating vein minerals, but disappear completely into barren parts of the quartz veins. All fluids are considered to have been generated by the F-rich Marviken granite (and related granite dykes), which show all geochemical criteria for an ore-fertile granite. The quartz veins investigated in the adjacent Svecofennian country rocks are considered to represent the very last stage of a fluid with similar characteristics to the fluid responsible for the ore formation in the Sarvlaxviken area, but that had cooled to <100°C.

Keywords: fluid inclusions, indium, polymetallic quartz veins, rapakivi granites, Sarvlaxviken, Finland.

Introduction

Interest in exploration for indium resources has been increasing world-wide (Schwarz-Schampera and Herzig, 2002), not least in Europe due to the significant dependence on supply for the high-technology electronics industry using this critical metal.

Indium rarely forms minerals of its own, but is usually enriched in the crystal structure of other minerals like sphalerite and chalcopyrite in polymetallic Cu- and Zn-sulfide deposits (Schwarz-Schampera and Herzig, 2002) and is typically closely related geochemically with Sn-bearing minerals in sulfide deposits (Qian *et al.*, 1998). High indium concentrations in sphalerite from

*E-mail: krisun@utu.fi
https://doi.org/10.1180/minmag.2017.081.024

This paper is part of a special issue entitled 'Critical-metal mineralogy and ore genesis'. The K.H. Renlund Foundation, Finland has contributed to the costs of Open Access publication for this paper.

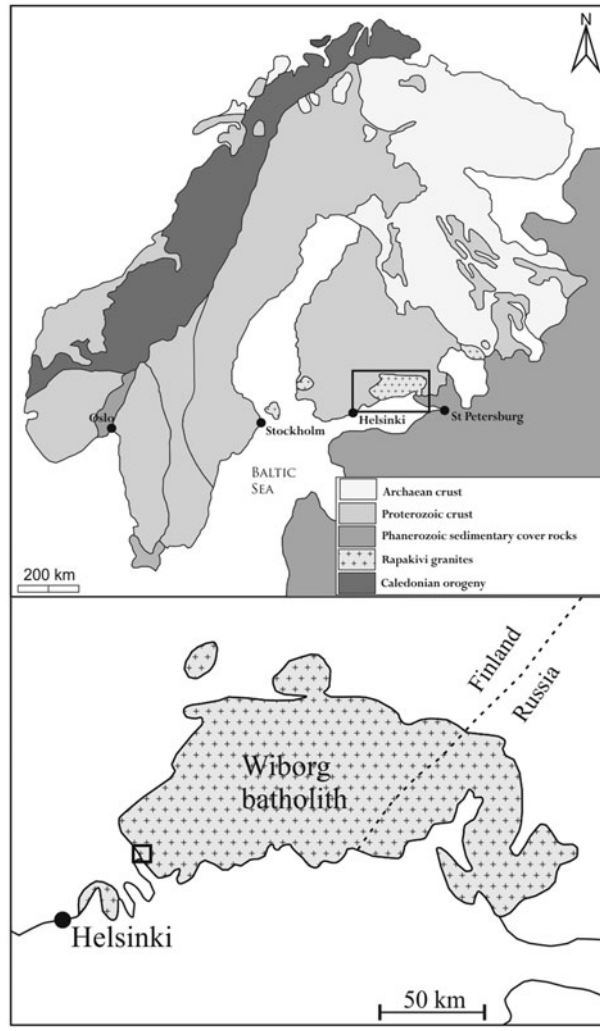

FIG. 1. Location of the Wiborg Batholith within the Fennoscandian Shield. The Sarvlaxviken area is indicated with a square in the western part of the Wiborg Batholith.

Sn-rich polymetallic ores are reported commonly worldwide e.g. from Freiberg in Germany, Mt. Pleasant, New Brunswick in Canada and Goka in Japan (Seifert and Sandmann, 2006).

Indium-bearing polymetallic veins have also been discovered in southern Finland (Fig. 1), mainly in the Sarvlaxviken area in the anorogenic 1.64 Ga Wiborg rapakivi batholith (Cook *et al.*, 2011; Valkama *et al.*, 2016*b*) but also in the adjacent 1.90 Ga Svecofennian crust (Villar *et al.*, 2016; Villar, 2017). The structurally controlled quartz veins in the Sarvlaxviken area are exceptional for the high indium contents, presence of roquesite and very high indium contents in sphalerite and chalcopyrite (Cook *et al.*, 2011).

The purpose of this investigation is to use fluid inclusion data on the indium-bearing polymetallic quartz veins in the Sarvlaxviken area in order to identify a depositional model for these veins and to bring new data and an overall insight into the genesis of indium-bearing vein deposits in anorogenic rapakivi granites. It is evident already from the studies of Cook *et al.* (2011); Valkama *et al.* (2016*a*,*b*); Villar *et al.* (2016) and Villar (2017) that the exploration potential for indium is huge in all rapakivi areas of the Fennoscandian Shield.

Geological background

The Fennoscandian Shield (Fig. 1) is a Precambrian multi-orogenic crustal complex in northern Europe, which consists of 3.1–2.6 Ga Archaean crust in the northeast and 2.5–0.9 Ga Proterozoic crust in the central and southwestern parts (Gaál and Gorbatschev, 1987). One of the most significant pieces of the Proterozoic crust was formed during the Svecofennian, when 1.92–1.89 Ga juvenile suspect terranes formed off-shore an Archaean continent. These exotic fragments collided subsequently with the Archaean continent and resulted in a series of metamorphic events of which the last one created anatectic melts and formation of 1.80–1.84 Ga Late Svecofennian granites (Gaál and Gorbatschev, 1987). Anorogenic rapakivi granites were emplaced as batholiths and stocks into the Svecofennian crust during the Mesoproterozoic of which the 1.65–1.63 Ga Wiborg Batholith (Fig. 1), in the south-eastern part of the shield, is the oldest and largest (Vaasjoki *et al.*, 1991; Rämö and Haapala, 2005).

The Sarvlaxviken area is located in the south-eastern part of the Fennoscandian Shield, ~90 km east of Helsinki, Finland, along the western margin of the Wiborg Batholith (Figs 1 and 2). The Svecofennian crust in that area is dominated by 1.84 Ga Late Svecofennian anatectic microcline granites (Kurhila *et al.*, 2011). The microcline in these Late Svecofennian granites has been altered thermally to orthoclase in a 10–20 km narrow zone along the intrusive margin of the Wiborg Batholith, when this rapakivi granite complex was emplaced into the Svecofennian crust (Vorma, 1972; Villar *et al.*, 2016). The Wiborg Batholith is dominated by wiborgite, a spectacular coarse-grained granite type, with 1–3 cm sized rounded orthoclase phenocrysts, mantled by a rim of plagioclase, within an even-grained groundmass of quartz, plagioclase, orthoclase, biotite and occasional hornblende (Simonen and Vorma, 1969). Other

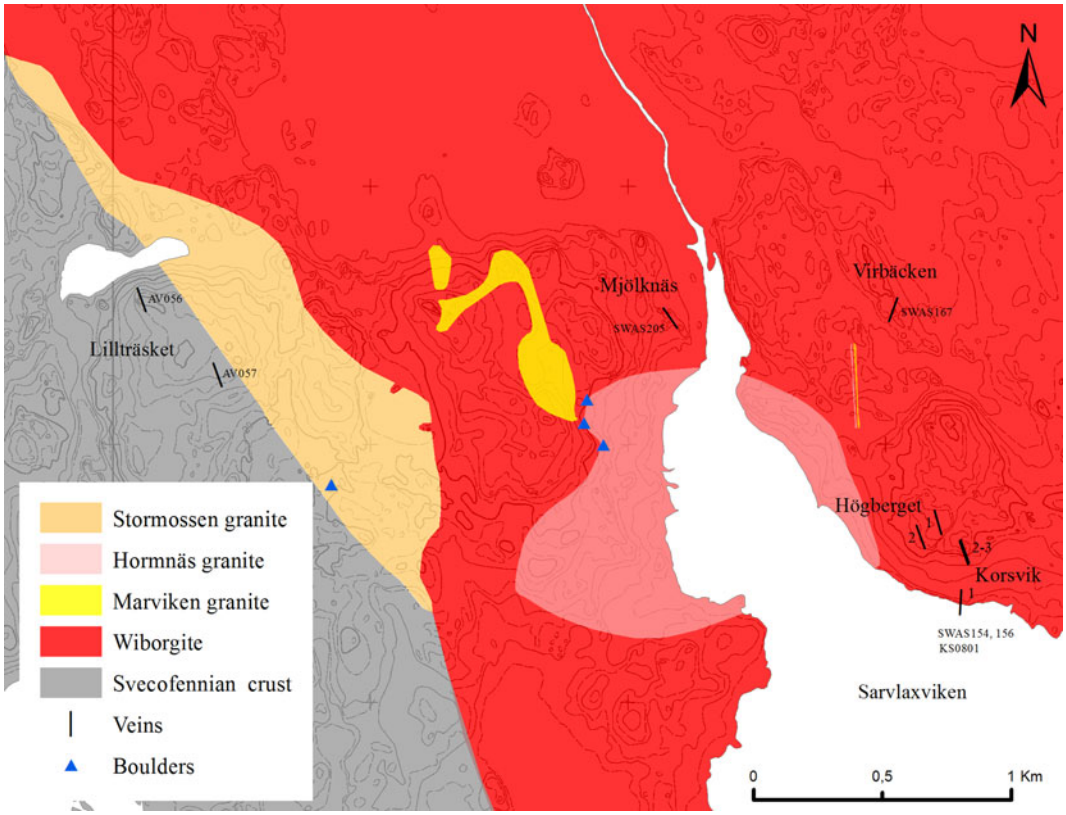

FIG. 2. Distribution of granite types, veins and ore boulders in the Lillträsket-Sarvlaxviken area. Sample numbers are indicated for the Lillträsket, Mjölknäs, Virbäcken and Korsvik-1 veins.

rapakivi granite varieties in the Sarvlaxviken area include the Hormnäs, Stormossen and Marviken granites, which constitute <1 km even-grained stocks and dykes, all representing later intrusion stages than the wiborgite, but still belonging to the Wiborg Batholith (Nygård, 2016).

The igneous components in the Wiborg Batholith are typical A-type granites with a pronounced within-plate granite character; the wiborgites have chondrite-normalized rare-earth element (*REE*) fractionation patterns with significant negative Eu anomalies and enrichments in light rare-earth elements (*LREE*) compared to the heavy rare-earth elements (*HREE*), while the later (topaz-bearing) granites display even more pronounced negative Eu anomalies and have fairly flat chondrite-normalized *REE* fractionation trends (Rämö and Haapala, 2005). The individual granite types in the Sarvlaxviken area are no exceptions to this (Nygård, 2016); the wiborgite in the Sarvlaxviken area shows all the geochemical characteristics of the wiborgites elsewhere in the batholith, including similar chondrite-normalized *REE* fractionation patterns and low Rb/Ba ratios (~0.2) while the Hormnäs, Stormossen and Marviken granites (Fig. 2) display significantly different contents of these elements. The Marviken granite is the most extreme of them, with pronounced enrichments of the *HREE* and very high Rb/Ba ratios (~14), thus having typical characteristics of an ore-fertile magma (Nygård, 2016). A N-S trending porphyric granite dyke, with a similar geochemical pattern to the Marviken granite, cuts the wiborgite on the north-eastern side of the Sarvlaxviken bay, parallel with the polymetallic quartz veins at Korsvik, Högberget, Virbäcken and Mjölknäs, a few hundreds of metres east and west of the porphyric dyke respectively.

Polymetallic vein deposits, of various styles and host rocks, have been discovered recently in the Sarvlaxviken area (Fig. 2); quartz veins in wiborgite at Korsvik, Högberget, Mjölknäs and Virbäcken (Cook *et al.*, 2008, 2011; Valkama *et al.*, 2016*b*), two types of alteration assemblages in the Marviken granite (Valkama *et al.*, 2016*b*) and a third type of alteration assemblage in the orthoclase-altered parts of the Late Svecofennian granite, <1 km from the intrusive contact of the Wiborg Batholith (Villar *et al.*, 2016; Villar, 2017). All vein types, also those in the Late Svecofennian granite, are considered to have formed from the late-stage rapakivi granites (Valkama *et al.*, 2016*b*; Villar *et al.*, 2016; Villar, 2017).

The wiborgite-hosted polymetallic deposits occur in three distinct generations (#1, #2a, #2b) of NNE- to NNW-trending quartz veins (Valkama *et al.*, 2016*b*). Most parts of the veins consist of quartz, with minor amounts of dark mica, chamosite and fluorite. Sulfide and/or oxide opaque minerals occur irregularly and are locally the dominant vein minerals for a few metres along strike. The oldest veins (generation #1) constitute the Högberget type, characterized by a 5 cm distinct alteration halo around the 0.5 cm thick quartz vein and a Li-As-W-Zn-dominated metal association. The ore minerals are principally arsenopyrite with smaller amounts of sphalerite and chalcopyrite, together with minor bornite, molybdenite, cassiterite, pyrite, galena and wolframite. The Mjölknäs type is characterized by a Pb-Zn-dominated metal association, represented by galena and sphalerite, and was also considered to belong to generation #1 by Valkama *et al.* (2016*b*) although there are no crosscutting relations to other vein generations to support this statement. Veins belonging to generation #2a (Virbäcken type) and #2b (Korsvik type) have been distinguished from generation #1 (and from each other) based on crosscutting field relations; vein generation #2a has generally a NNE trend while the dominating trend for vein generation #2b is NNW. Furthermore, the two vein generations (#2a and #2b) also show variations in the metal contents although both are characterized by a Cu-As-In-dominated metal association; the Ag grades are distinctly higher in generation #2a and the In grades increase from generation #1 (0–100 ppm), via generation #2a (40–150 ppm) to generation #2b (600–1500 ppm). The ore minerals are dominated by chalcopyrite with smaller amounts of arsenopyrite and sphalerite together with minor roquesite, pyrite, cassiterite, stannoidite, bornite, galena, wolframite and Bi-minerals (Valkama *et al.*, 2016*b*).

A paragenetic summary of the opaque phases in the Högberget (generation #1), Virbäcken (generation #2a) and Korsvik (generation #2b) veins is presented in Fig. 3, showing increasing abundance of chalcopyrite, cassiterite, wolframite and roquesite, but decreasing abundance of molybdenite, sphalerite, galena and silver minerals through time. This can also be seen in the metal contents in these veins, reported by Valkama *et al.* (2016*b*); increasing contents of Cu, Sn, W and In, but decreasing contents of Mo, Zn, Pb and Ag through time. From a structural perspective, the fractures hosting vein generations #2a and #2b are considerably more brittle than the fractures hosting vein generation #1, indicating more shallow deposition levels with time. In consequence, if the paragenetic, geochemical and structural observations are matched with each other, we see a contradictory, or even chaotic,

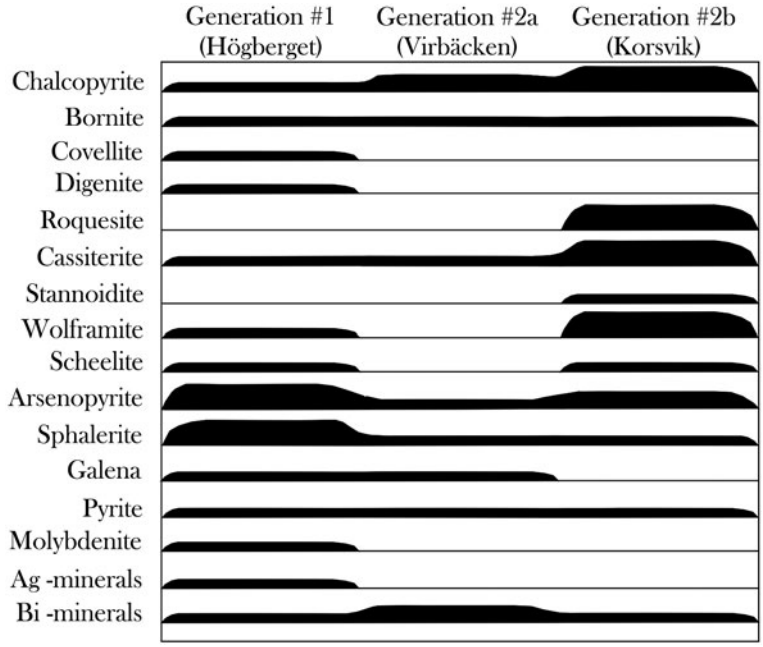

FIG. 3. Paragenetic summary of the opaque phases in the Högberget (generation #1), Virbäcken (generation #2a) and Korsvik (generation #2b) veins.

zonation pattern with respect to where in the vein system each metal precipitated.

Positive evidence for intense ore-forming processes in the Marviken granite and in the Late Svecofennian granites, the latter immediately west of the Wiborg Batholith, exist through discoveries of numerous local boulders with metal enrichments as well as extensive and complex soil anomalies with respect to a number of metals, but sulfide-bearing veins in outcrop have so far not been located in these granites. The occurrences of metal-rich veins in the Marviken granite can, according to studies of the ore-bearing boulders, be divided into a Cu-As-Sn-dominated type in 1–3 cm thick zones of greisen alteration assemblages and a Mo-Bi-dominated type in a 20–30 cm thick zone in a Be-rich alteration assemblage (Valkama *et al.*, 2016*b*). Metal enrichments in the Late Svecofennian granite have also been revealed south of Lake Lilltträsket, where a 50 cm wide Zn-rich alteration zone in a granite boulder has been found associated with a widespread and complex geochemical soil anomaly (with respect to Zn, Cd, In, Ag, Fe, Pb, Bi and As). A short (<20 m) glacial transport distance from the bedrock source has been suggested for these soil anomalies, based on detailed ground magnetic anomaly patterns (unpublished data) and susceptibility data, partly on the bedrock and partly in the same soil samples in which the geochemical anomalies were detected (Vind, 2014). The metal-rich soil anomalies occur where the Late Svecofennian granite is part of the thermal alteration zone that Vorma (1972) identified for the transfer of microcline into orthoclase outside the Wiborg Batholith. This thermal alteration is accompanied by widespread hydrothermal potassic alteration in the Lilltträsket area, which led Villar *et al.* (2016) and Villar (2017) to conclude that metal enrichments in the concealed bedrock must be located in the Late Svecofennian granite, <1 km from the intrusive margin of the Wiborg Batholith.

Sample material

Fourteen samples of hydrothermal 0.5–2 cm thick vein quartz and associated ore minerals have been collected for the present study. Sample numbers, vein name and coordinates are summarized in Table 1. All samples were carefully selected in order to provide a meaningful relation between the fluid inclusion data from the quartz (and/or fluorite/cassiterite) and the precipitation conditions for the opaque minerals. Most of the samples investigated

TABLE 1. Fluid inclusion samples.

Vein/reference	Generation #	Sample	Host mineral	Coordinates*
Högberget 1[a]	#1	KS1401	Qtz, Fl	3455358E 6700517N
Högberget 1[a]	#1	KS1402	Qtz	3455355E 6700527N
Högberget 2[a]	#1	KS1406	Qtz	3455287E 6700453N
Mjölknäs[b]	#1?	SWAS 205	Qtz	3454314E 6701301N
Virbäcken[b]	#2a	SWAS 167	Qtz, Cst, Fl	3455182E 6701334N
Korsvik 1[b,c]	#2b	KS 0801	Qtz	3455444E 6700200N
Korsvik 1[b,c]	#2b	SWAS 154	Qtz, Fl	3455444E 6700200N
Korsvik 1[b,c]	#2b	SWAS 156	Qtz, Fl	3455444E 6700200N
Korsvik 2[b,c]	#2b	SWAS 147-150	Qtz, Fl	3455455E 6700392N
Korsvik 3[b]	#2b	SWAS 158	Qtz	3455458E 6700397N
Korsvik 3[b]	#2b	SWAS 159	Qtz, Fl	3455458E 6700397N
Korsvik 4[a]	#2b	KS 1405	Qtz	3455290E 6700453N
Lillträsket[d]	#3	AVO 56	Qtz	3452259E 6701373N
Lillträsket[d]	#3	AVO 57	Qtz	3452555E 6701081N

References: a = this study, b = Valkama *et al.* (2016*b*), c = Cook *et al.* (2011), d = Villar (unpublished data). Qtz = quartz, Fl = fluorite, Cst = cassiterite.
*Coordinates E/N in the Finnish national grid system.

in the present study (Korsvik, Virbäcken and Mjölknäs) are those for which Cook *et al.* (2011) and Valkama *et al.* (2016*b*) made their observations of ore minerals. This implies that the fluid inclusion data in this study have been obtained mainly from quartz (and/or fluorite/cassiterite) grains at distances of mm to cm from the ore minerals (or even intergrown with them), regardless of the In grades. The only vein for which larger distances exist between quartz investigated for fluid inclusions and abundant opaque minerals is the Högberget-1 vein where the fluid inclusion samples (KS1401 and KS1402) were taken at a distance of 10–20 m along strike and in the same vein, from where Valkama *et al.* (2016*b*) reported intense occurrence of ore minerals (Figs 4 and 5*a*). Sample KS1406 was collected in another quartz vein (Högberget-2; generation #1), 80 m WSW of the Högberget-1 vein. The sample location for KS1406 is at a distance of 1 m from sample EN1329, for which Valkama *et al.* (2016*b*) reported high Li, W and As contents. The sample of the Mjölknäs vein, generation #1 (SWAS 205), is identical to the sample documented by Valkama *et al.* (2016*b*).

Samples representing generation #2a; SWAS 167 (the Virbäcken vein) and generation #2b; KS0801, SWAS 154, SWAS 156, SWAS 147-150, SWAS 158 and SWAS 159 (the Korsvik veins) are also the same as those in which Cook *et al.* (2011) and Valkama *et al.* (2016*b*) reported abundant ore minerals. Sample KS 1405 was collected from a quartz vein that belongs to generation #2b, cutting and faulting the Högberget-2 vein (belonging to generation #1, see Figs 4 and 5*b*). Since all metal-rich veins in the Marviken and Late Svecofennian granites are hosted by various types of alteration assemblages (and not in proper quartz veins), it was not possible to collect adequate hydrothermal minerals for fluid inclusion studies from the Marviken and Lillträsket areas. Instead, two barren hydrothermal quartz vein samples (generation #3), assumed to represent the rapakivi-induced epigenetic metal-enriched environment in the Late Svecofennian granite, were sampled south of Lake Lillträsket (AVO 56 and AVO 57).

Analytical techniques

The samples were prepared at the University of Turku as doubly-polished 150 µm thick sections (Fig. 6) for fluid inclusion observation and analysis. A conventional petrographic microscope was used to get an overview of the samples and the distribution of fluid inclusions. The microthermometric analyses were performed with a Linkam THM 600 heating/freezing stage (working range −196 to +600°C) adapted for a Nikon microscope at the Department of Geological Sciences, Stockholm University. Calibration was made with commercial SynFlinc® synthetic fluid inclusion standards. Phase transitions of fluid inclusions were observed with a 40× long-working distance objective. The

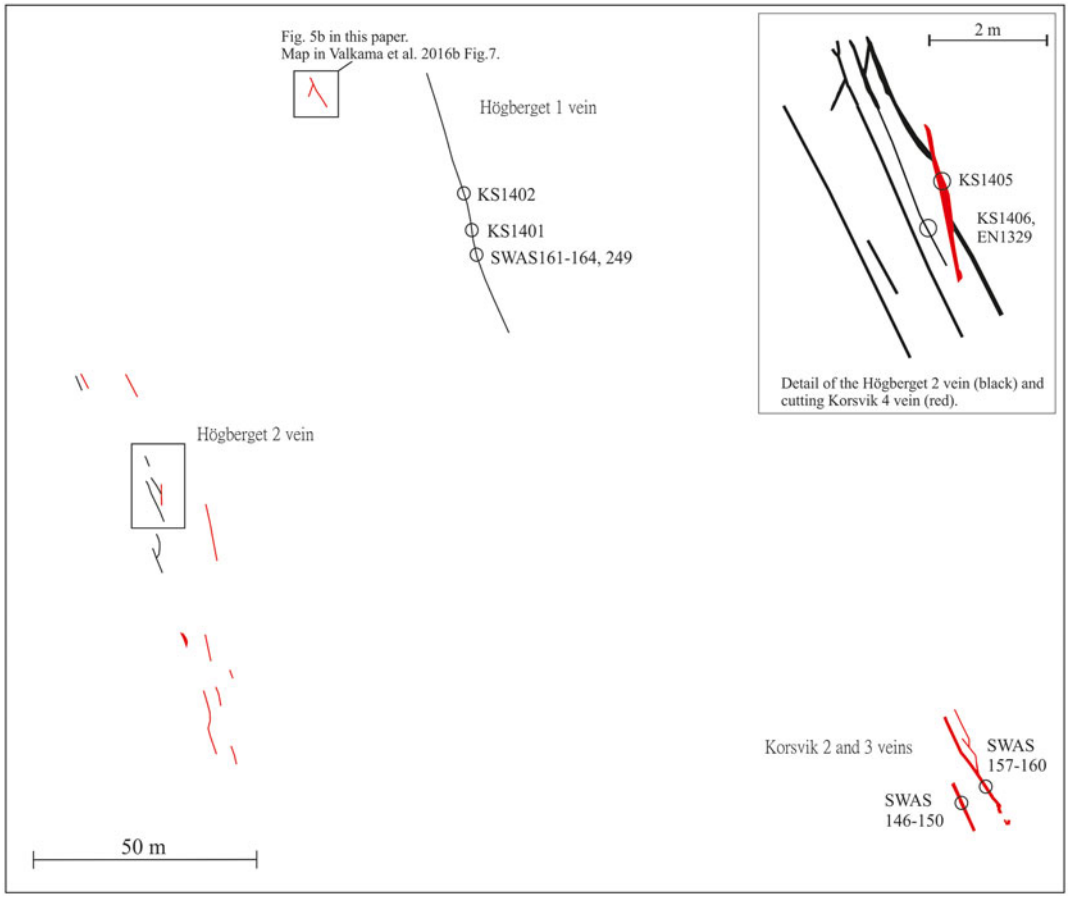

FIG. 4. Spatial relations between the polymetallic quartz veins in the Högberget-Korsvik area with sample numbers indicated for the Högberget-1 and -2 veins as well as the Korsvik -2, -3 and -4 veins. Black lines represent the Högberget type (generation #1) and the red lines the Virbäcken and Korsvik types (generations #2a and #2b).

accuracy of the measurements is estimated to be ±0.1°C for temperatures below +30°C and ±1.0°C for higher temperatures. Fluid inclusions with evidence of leakage or necking down were not analysed. Salinities of aqueous fluid inclusions were calculated after data in Bodnar (2003) while determination of salinities from gas hydrate dissociation temperatures in CO_2-bearing aqueous inclusions was made after data in Bakker *et al.* (1996).

Fluid inclusion studies

To obtain an adequate documentation of the fluids involved in the formation of both the ore and the gangue minerals (most ore minerals are not suitable for conventional microthermometric analysis), fluid inclusions were studied on quartz, either associated spatially with the ore minerals or where it is the dominating vein mineral and more rarely on occasional cassiterite and fluorite grains. Fluid inclusions in all samples belonging to all vein generations (#1, #2a, #2b and #3), have a random three-dimensional distribution in the host minerals and were classified as primary fluid inclusions according to Roedder (1984). The sizes of the inclusions are in general <10 μm, but can reach 35 μm in quartz, 20 μm in cassiterite and 45 μm in fluorite. The inclusions in vein generations #1, #2a and #2b consist mainly of an aqueous liquid and a vapour (Fig. 7*a*,*b*,*c*), but in a few quartz-hosted inclusions there is also an additional carbon dioxide component in the vapour phase (Fig. 7*d*). The inclusions in quartz and cassiterite appear with variable proportions of the liquid and the vapour

FIG. 5. (*a*) The Högberget-1 vein, representing generation #1, photographed towards N by Jeremy Woodard (with Nadya Priyatkina as scale) on the site where sample KS 1402 was collected. (*b*) Cutting relations between quartz veins representing generations #2a and #2b at Högberget (photo modified after Valkama *et al.*, 2016*b*).

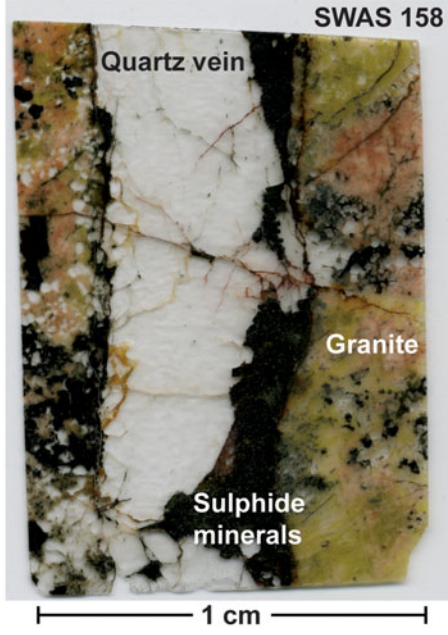

FIG. 6. Doubly polished thick section of sample SWAS 158 from the Korsvik-3 vein (generation #2b), with sulfide/oxide minerals deposited along the contact to the host granite.

phase (from 5 to almost 90 vol.% vapour), whilst the inclusions in fluorite have constant phase ratios with ~5 vol.% vapour (Fig. 7*e*). The quartz-hosted fluid inclusions in the samples belonging to vein generation #3 are all liquid aqueous fluid inclusions.

Microthermometric results

The microthermometric results are presented in Table 2 and in Figs 8 and 9. The initial melting of ice (the temperature, at which first liquid is recognized during warming of frozen inclusions) was observed for all samples (except for the CO_2-bearing inclusions) in the interval from −22° to −30°C which indicate that NaCl and KCl are the most likely principal salts (Davis *et al.*, 1990) in the aqueous solution (even though smaller amounts of other salts such as $CaCl_2$ can be present). The initial melting temperature was observed for the majority of the inclusions between the metastable eutectic at −28°C and the stable eutectic at −22.9°C of the H_2O–NaCl–KCl system (Davis *et al.*, 1990). A composition dominated by $CaCl_2$, or other divalent cations, would give significantly lower initial melting temperatures (Davis *et al.*, 1990).

Final melting of ice in all aqueous inclusions hosted by vein quartz generation #1, #2a and #2b,

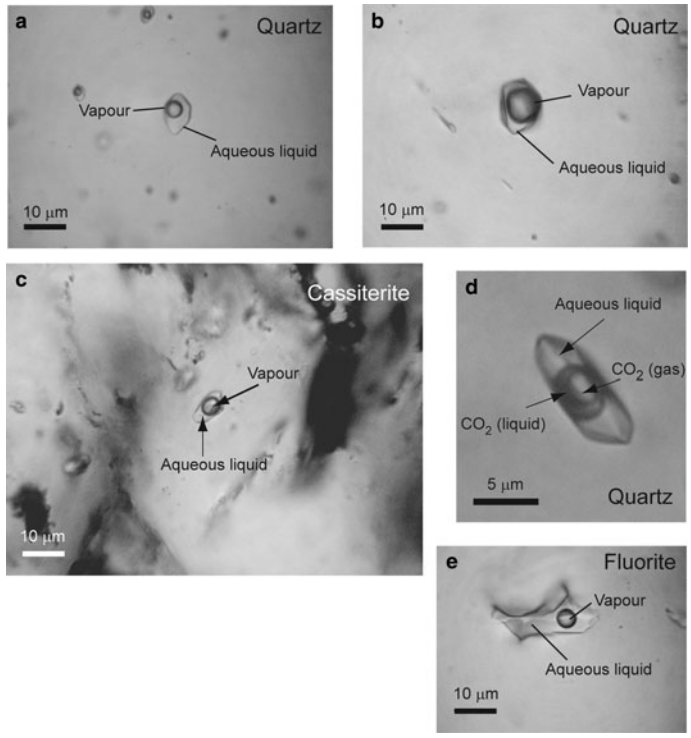

FIG. 7. (*a* and *b*) Quartz-hosted fluid inclusions with varying phase proportions. (*c*) Vapour-rich fluid inclusion in cassiterite. (*d*) CO_2-bearing aqueous fluid inclusions in quartz. (*e*) Aqueous fluid inclusions in fluorite.

took place in the range 0 to −12.3°C, which corresponds to salinities of 0–16.2 eq. mass% NaCl. Dissociation of gas hydrates in the CO_2-bearing aqueous inclusions occurred between +4.0 and +7.1°C which correspond to a salinity of 5.0–8.0 eq. mass% NaCl. The measurements revealed no discernible differences between the quartz vein generations #1, #2a and #2b (Figs 8 and 9). Inclusions with low salinities dominate in all samples, but higher salinities are often recorded in metal-rich parts of the veins. The inclusions hosted by cassiterite show final ice melting temperatures of −3.0 to −5.8°C, corresponding to salinities of 4.9–8.9 eq. mass% NaCl. Fluid inclusions in fluorite have final ice melting between −0.2 and −3.3°C and a salinity of 0.3–5.4 eq. mass% NaCl.

Total homogenization temperatures of fluid inclusions in quartz were recorded over a broad temperature interval from 73 to 410°C, including CO_2-bearing inclusions, with homogenization both to the liquid and vapour state. Cassiterite shows a similar range of homogenization temperatures to liquid and vapour from 111 to 519°C. Fluorite has a more limited range of temperatures from 123 to 169°C with homogenization to liquid in all cases.

Partial homogenization of the CO_2 in the few aqueous CO_2-bearing inclusions occurred at +20.6 to +28.2°C to liquid and vapour. Melting of the CO_2 was observed between −56.9 and −57.2°C, indicating an almost pure CO_2 phase with less than 3 mol.% CH_4 or N_2 (based on data from van den Kerkhof and Thiéry, 2001).

The fluid inclusions in the quartz vein samples from the Lillträsket area (generation #3) lack a gas bubble and, therefore, it was not possible to obtain a homogenization temperature, but this type of inclusion is assumed to have been trapped at temperatures below ~100°C (Roedder, 1984). The salinity of aqueous inclusions is normally calculated from the ice melting temperature of two-phase liquid and vapour inclusions, but to avoid metastable ice melting in these all-liquid inclusions (Roedder, 1984), final ice melting temperatures were measured after inducing an artificial vapour bubble in the inclusions by heating and stretching them. After this treatment they displayed final ice melting temperatures between −0.3 and −0.6°C

TABLE 2 Microthermometric data from Sarvlaxviken.

Vein generation	Sample	Host mineral	Th (°C)	Tm (°C) −/+ = ice or CO_2 hydr	Salinity (eq. mass% NaCl)	$ThCO_2$ $TmCO_2$ (°)
#1	KS1401	Qtz	100 to 280 L	−0.8 to −11.1	1.4 to 15.1	–
		Fl	123 to 149 L	−3.0 to −3.3	5.0 to 5.4	
#1	KS1402	Qtz	144 to 209 L	0.0 to −8.0	0.0 to 11.7	–
#1	KS1406	Qtz	141 to 263 L	−2.7 to −10.3	4.5 to 14.3	21.2 to 28.8 V
		Qtz	257 to 294 V	+4.0 to +5.1	7.3 to 8.0	−56.9 to −57.0
#1?	SWAS205	Qtz	94 to 309 L	−0.5 to −9.6	0.9 to 13.5	–
		Qtz	241 to 330 L	+4.0 to +8.0	4.5 to 11.0	
#2a	SWAS167	Qtz	115 to 331 L	−0.5 to −9.2	0.9 to 13.1	25.6 L
		Qtz	334 V	+4.6	10.0	−57.2
		Cst	111 to 384 L	−3.0 to −5.8	4.9 to 8.9	
		Cst	330 to 519 V	−3.0 to −3.3	4.9 to 5.4	
		Fl	134 to 143 L	−0.2 to −1.2	0.3 to 1.9	
#2b	KS0801	Qtz	102 to 271 L	−2.2 to −12.3	3.7 to 16.2	–
#2b	SWAS154	Qtz	73 to 174 L	−1.2 to −4.8	2.1 to 7.6	–
		Qtz	350 to 410 V	−3.0 to −3.6	4.9 to 5.9	
		Fl	134 to 145 L	−1.0 to −1.1	1.7 to 1.9	
#2b	SWAS156	Qtz	111 to 309 L	−2.9 to −8.5	4.8 to 12.3	–
#2b	SWAS147-150	Qtz	203 to 296 L	+6.7 to +7.1	5.0 to 5.1	20.6 to 28.2 L
		Fl	122 to 152 L	−0.7 to −1.4	1.2 to 2.4	−56.9 to −57.0
#2b	SWAS158	Qtz	130 to 272 L	−0.4 to −1.4	1.4 to 2.4	–
#2b	SWAS159	Qtz	86 to 297 L	−0.3 to −11.5	0.5 to 15.5	–
		Fl	159 to 169 L	−0.8	1.4	
#2b	KS1405	Qtz	155 to 272 L	−0.6 to −1.3	1.1 to 2.2	–
		Qtz	340 V	−0.6	1.1	
#3	AVO56	Qtz	<100 (all liquid FI)	−0.3 to −0.6	0.5 to 1.1	–
#3	AVO57	Qrtz	<100 (all liquid FI)	−0.3 to −0.6	0.5 to 1.1	–

L = homogenization to the liquid state, V = homogenization to the vapour state.

which correspond to salinities in the range 0.5–1.1 eq. mass% NaCl (Fig. 9).

Discussion

The ore-forming conditions in the Sarvlaxviken area

The fluid inclusion data for the veins in the Sarvlaxviken area demonstrate that the mineralizing fluid that entered the fractures in the wiborgite was a low- to moderately-saline aqueous fluid. A few randomly occurring inclusions enclose an additional pure CO_2 phase, which implies that the aqueous fluid initially contained some CO_2. Magmatic fluids commonly contain CO_2 as one of the volatile components (Heinrich, 2005) and fluid inclusions in In-enriched vein deposits have been reported to include CO_2 together with an aqueous low- to moderately-saline fluid (Schwarz-Schampera and Herzig, 2002; Moura *et al.*, 2014). However, the significance of the CO_2 phase is not completely established, but the appearance of a CO_2 phase in a few inclusions, and not in all, suggests that the CO_2 has separated and escaped from an originally homogenous H_2O–CO_2 fluid, a process that is known to occur in response to the rapid cooling and a pressure decrease (Wilkinson, 2001). Furthermore, the presence of fluorite and sulfides in the veins demonstrates that the metal-transporting fluid also carried F and S.

Even if it had been possible to distinguish between three distinct generations of ore-bearing quartz veins in the Sarvlaxviken area, the paragenetic sequences (Fig. 3) and metal associations (Valkama *et al.*, 2016*b*) show complex and ambiguous zonation patterns with respect to time and assumed depositional levels in the crust. The

first vein generation (#1), which also represents the deepest deposition level, has the highest Zn and Pb contents (as well as significant W grades). The second vein generation (#2a) shows the highest Ag grades, while the third vein generation (#2b) that is associated with brittle fracturing at a presumed high crustal level has the highest contents of Cu, Sn and W, metals that normally form in the bottom of a complex vein system. The fluid inclusion data support this chaotic system; there are no clear temperature gradients when moving from generation to generation. Instead, the fluid inclusion data from the three vein generations #1, #2a and #2b are indistinguishable and indicate that the same fluid was involved in all three generations.

The variable phase proportions in coexisting fluid inclusions suggest that the precipitation

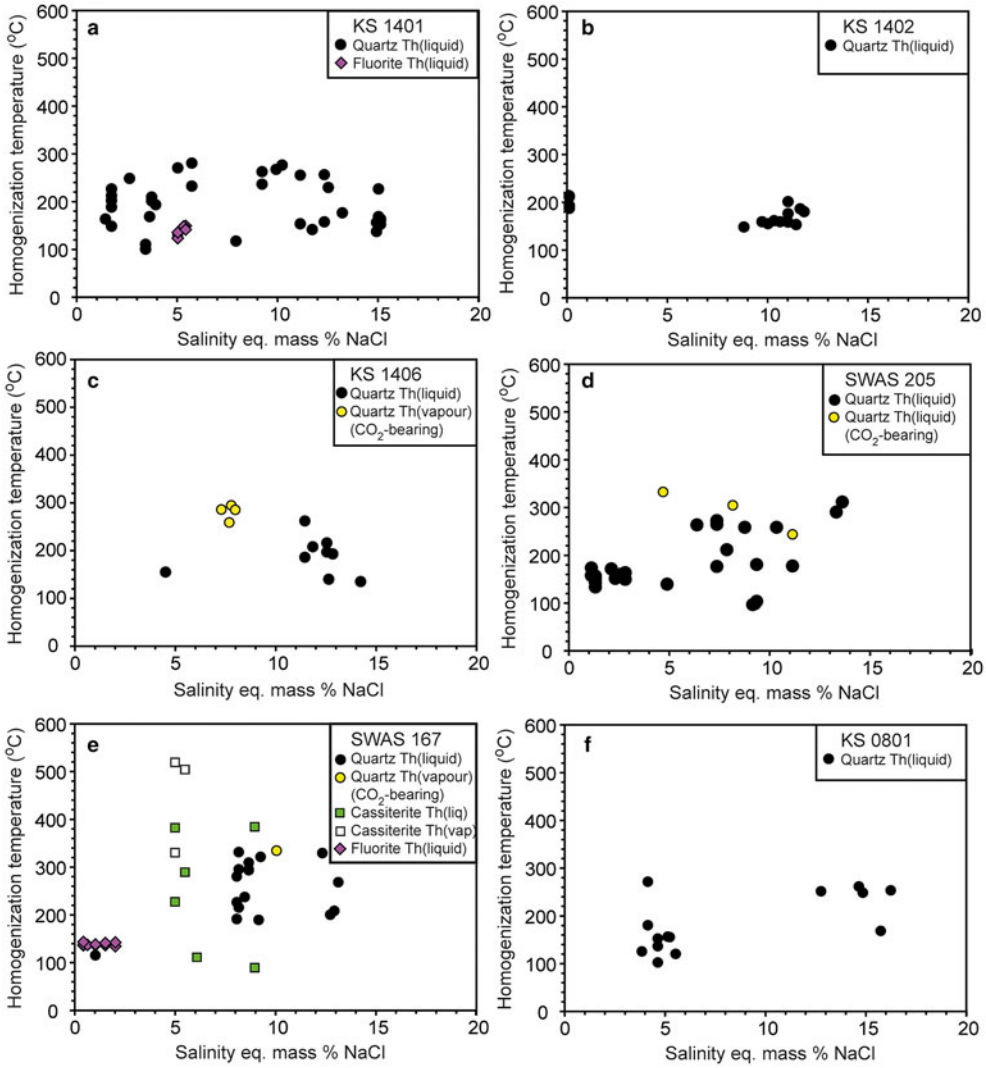

FIG. 8. Total homogenization temperatures (°C) plotted *vs*. salinity (eq. mass% NaCl) in fluid inclusions in quartz (circles), cassiterite (squares) and fluorite (diamonds) from the Sarvlaxviken veins. Diagrams (*a*) and (*b*) represent the Högberget-1 vein (generation #1), diagram (*c*) the Högberget-2 vein (generation #1), diagram (*d*) the Mjölknäs vein (generation #1?), diagram (*e*) the Virbäcken vein (generation #2a) while diagrams (*f*) to (*l*) represent the Korsvik veins (generation #2b). Further information about the samples is given in Table 1.

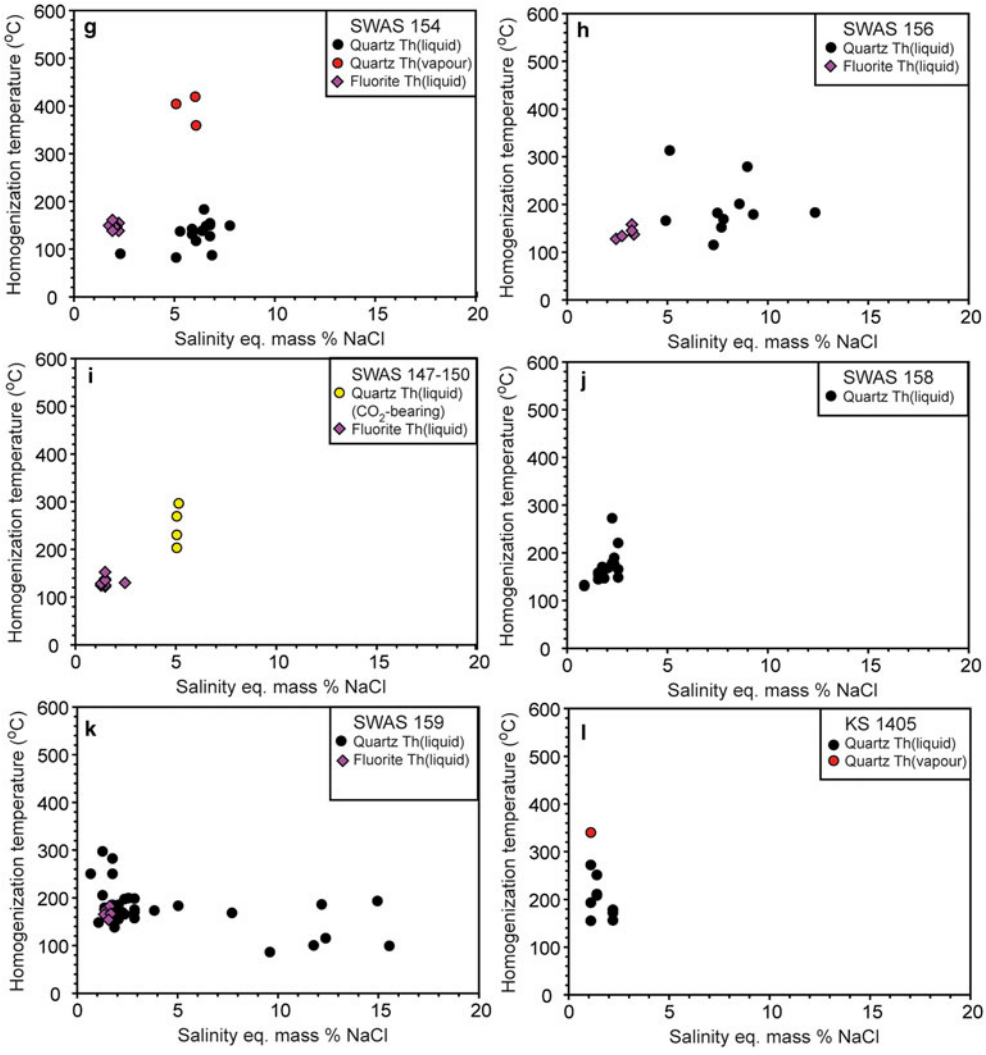

FIG. 8. Continued.

appears to have been very sudden and that the inclusions were sealed synchronously under heterogeneous conditions (Roedder, 1984; Wilkinson, 2001). The alternatives, that the fluid inclusions were affected by post-entrapment deformation related modifications (stretching and recrystallization; Audétat and Günther, 1999) with leakage and changes in shape and composition, or the inflow of some unrelated fluid, are not to be expected as the quartz veins are well preserved and not deformed. When volatiles exsolve from a magma in an early stage of immiscibility, a separate aqueous volatile-rich fluid is produced. Upon ascent, this aqueous phase commonly unmixes during a second stage of immiscibility into a highly saline (30–70 eq. mass% NaCl) liquid and a low-salinity (<10 eq. mass% NaCl) vapour phase (Bodnar *et al.*, 1985; Roedder, 1992; Heinrich, 2005). The salinities of the two phases depend on the actual *PT* conditions. Even though the salinities of the measured fluid inclusions of the Sarvlaxviken quartz veins span a wide range, no salinities were obtained above 16 eq. mass% NaCl. This suggests that the aqueous fluid trapped as inclusions represents the upward moving vapour phase after unmixing from a liquid, or an aqueous phase directly separated from a magma. The somewhat higher salinity (up to 16 eq. mass%

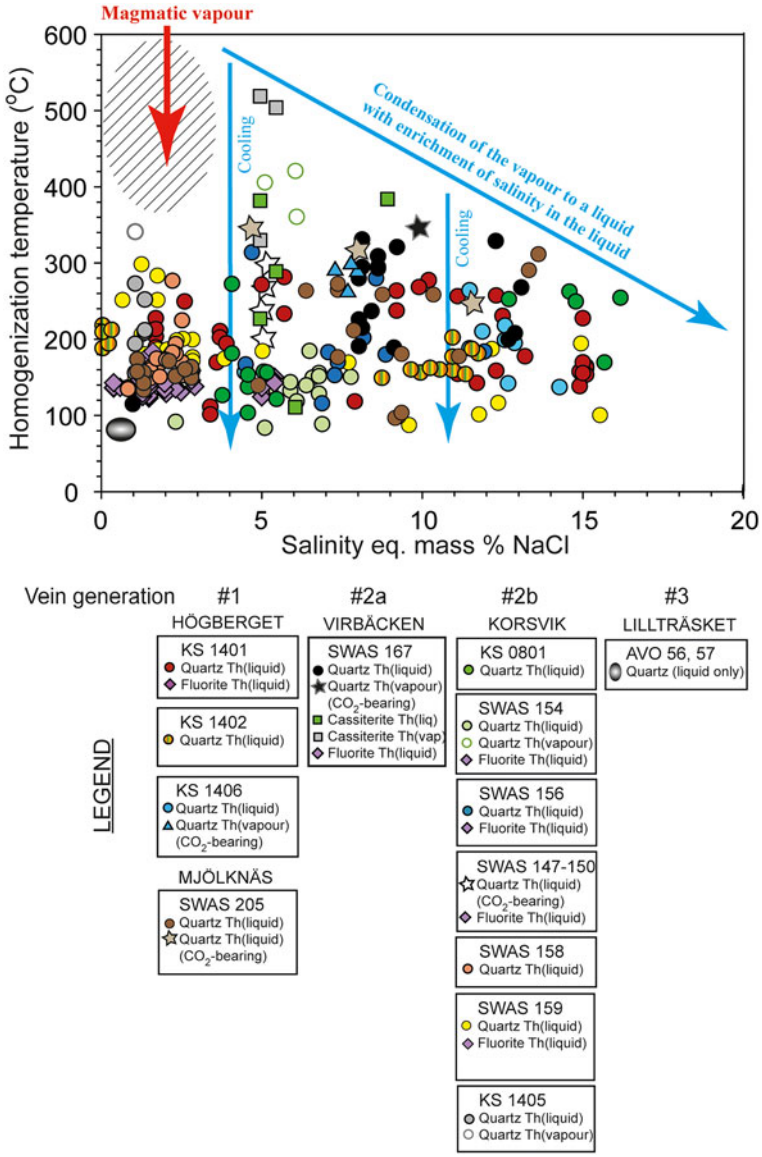

FIG. 9. A plausible interpretation of the homogenization temperatures and salinities obtained from this study. Hot vapour, exsolved from a magma, rises (red arrow) from depth along the fracture and interacts with the granite walls. Condensation, cooling and boiling of the vapour (blue arrows) result in a liquid with progressively higher salinity by continuous vapour-liquid separation.

NaCl), compared to what is usually reported (<10 eq. mass% NaCl) for the low-salinity vapour phase, and the spread in homogenization temperatures (~100 to ~500°C) may be explained by combined processes of phase separation involving condensation, cooling and boiling of an initially low-salinity (<3 eq. mass% NaCl) vapour (Fig. 9) during its ascent through the fractured granite. Discharge of the fluids along faults or fracture systems, associated with the magmatic activity, resulted in a conductive cooling of the vapour by interaction with the fractured wall rock. Decreased temperature by conductive cooling is an effective mechanism that

will lead to a decreased solubility and precipitation of the metals transported in the fluid (Heinrich, 2005).

At first, the aqueous fluid probably had a high temperature (500–600°C) and was exsolved during the last stage of magma crystallization (Fig. 10*a*). In response to fracturing (pressure decrease), liquid/vapour phase separation occurred and steam was formed that rose upwards in the fractures. It is generally believed (Schwarz-Schampera and Herzig, 2002; Seifert and Sandmann, 2006) that In-bearing deposits originate from magmatic systems and that it's moderate geochemical incompatibility during magma crystallization and the high volatility (Sun, 1982) eventually result in mobilization and transport of indium into the volatile-rich magmatic vapour. Hot magmatic vapour-like fluids can carry high concentrations of metals (Heinrich, 2005). High-temperature (500–900°C) fumaroles of water vapour derived from a degassing magma contain significant amounts of dissolved indium (Symonds *et al.*, 1987). The F contents in the rapakivi granites in the Sarvlaxviken area are (as elsewhere in the Wiborg Batholith; Rämö and Haapala, 1995, 2005) commonly in the range of 0.1–0.2 wt.% but on average ca. 0.5 wt.% in the Marviken granite (Nygård, 2016), the latter thus a significantly F-rich granite. Experimental studies have indicated a strongly depressed solidus, due to the presence of an F-rich melt, to temperatures from 700°C to a final stage of 500°C (Costi *et al.*, 2009).

As the temperature of the steam decreased adjacent to the contact with the fracture walls (Fig. 10*b*), droplets of a higher density liquid phase separated. Initially, at still relatively high temperatures, small portions of this liquid were carried as droplets in the ascending dispersed vapour flow, but with decreasing temperatures the droplets formed a descending liquid layer which became saturated with metals that started to precipitate where the concentration of salt increased. The salinity rose rapidly along the granite wall while salt-free water boiled off and passed upwards as steam, the process continued with a cooling/heating cycle with condensation of new droplets that fell back down the fracture where water was reheated and boiled off, like circulation in a steam engine. The highest salinities were recorded in fluid inclusions in metal-rich parts of the veins. Combined condensation and boiling of an aqueous liquid from a vapour phase is an effective mechanism for producing high-salinity fluids (Roedder, 1984). The vapour flow continued in the centre of the fracture, but was blocked near the fracture walls by the liquid condensate and the

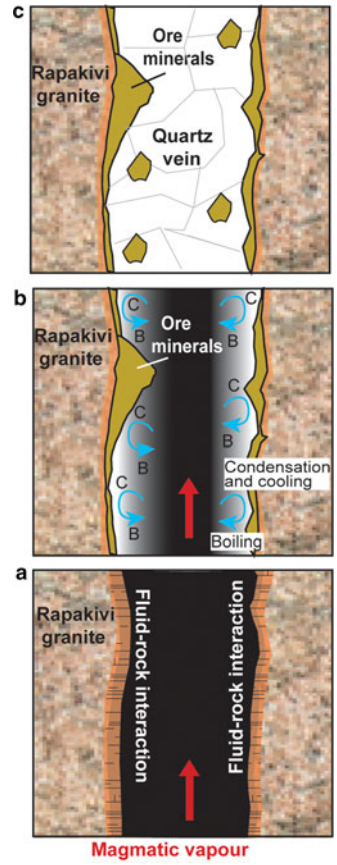

FIG. 10. Simplified model for the formation of the Sarvlaxviken polymetallic quartz veins; (*a*) Vapour exsolved from a magma rises from depth (red arrow), interacts and alters the walls of the fractured wiborgite. (*b*) Cooling of the ascending hot magmatic vapour along the fracture walls (blue arrows) leads to contact condensation into liquid water, reheating, boiling and subsequent cooling of the liquid phase (C = condensation and cooling, B = boiling) with a progressive increase in concentration of salt and metal components. Ore minerals are deposited. (*c*) The open fracture is finally filled and sealed by quartz.

precipitated ore minerals and quartz (Fig. 10*b*). Finally, the fractures were sealed by quartz at which point the fluid flow ceased (Fig. 10*c*). Condensation, cooling and boiling of the vapour resulted in a turbulent flow with complex geometry and a temperature-salinity pattern which was reflected by the variable liquid-to-vapour proportions and salinities in the fluid inclusions. Published data of metal concentration in fluid inclusions from

a variety of ore deposits show that different metals preferentially concentrate either in the liquid (e.g. Zn, Fe, Sn, Pb) or in the vapour phase (e.g. Cu, As) depending on whether they can be transported in the liquid as Cl-complexes or in the vapour as sulfur (HS)-complexes (Heinrich *et al.*, 1999). This may explain the irregular metal enrichments observed by Valkama *et al.* (2016*b*) in the Sarvlaxviken veins. The quartz veins in the Lillträsket area were also formed from late-stage granite activity, but at the very last stage of vein formation (thus considered to represent a generation #3) from a cool (<100°C) and low-salinity (<1 eq. mass% NaCl) aqueous fluid. The investigated quartz veins at Lillträsket are late and the fluid inclusion data can therefore not really be considered to reflect the conditions for the main widespread ore-mineralizing system in that area. However, it is instead highly likely that the fluids that were responsible for the metal concentration processes in the Lillträsket area were very similar to the fluids described for the three generations of polymetallic quartz veins in the Sarvlaxviken area. This assumption is also very realistic for the metal-enriched systems in the Marviken granite. This granite is by far the most F-rich granite in the area (and also displays other ore-fertile geochemical criteria like a high Rb/Ba ratios and characteristic inclined *HREE* pattern) and has a high potential to be a source for the necessary F-rich fluids. The fact that a granite dyke, with Marviken geochemical characters (high F contents, high Rb/Ba ratios and an inclined *HREE* pattern), exist on the eastern side of the Sarvlaxviken bay, parallel with adjacent polymetallic quartz veins, provides further support for a link between the Marviken granite (and associated dykes) and the ore-forming fluids responsible for the Sarvlaxviken quartz veins and the alteration dominated veins in the Lillträsket and Marviken areas.

Comparison with other In-bearing deposits

Indium-bearing deposits appear in a large variation of sizes and ore types (Schwarz-Schampera and Herzig, 2002) such as polymetallic structurally controlled veins, complex granite-related vein-stockwork systems, volcanic-hosted massive Cu-Zn sulfide deposits, base-metal-rich porphyry copper deposits, skarn deposits, epithermal deposits and fumarole precipitates in active magmatic systems. Indium-rich deposits in polymetallic vein and complex granite-related vein-stockwork systems are among the most important types (Seifert and Sandmann, 2006).

The fluid inclusion data presented in this paper are basically similar to data for In-bearing vein-type deposits in Argentina, Bolivia, Canada, Germany and Japan (Schwarz-Schampera and Herzig, 2002; Seifert and Sandmann, 2006; Sinclair *et al.*, 2006; Jovic *et al.*, 2011; Shimizu and Morishita, 2012) with proposed formation temperatures in the range from ca. 200 to 400°C. Differing results were presented by Dill *et al.* (2013) who suggested significantly lower deposition temperatures (between 130 and 250°C) for the San Roque epithermal Au-Cu-Zn-Pb-Ag veins in Argentina. An extended temperature interval (from <200 to 450°C) was proposed by Moura *et al.* (2014) for the Mangabeira Sn-In deposit in Central Brazil, which is more in conformity with the Sarvlaxviken data.

Based on the composition of condensates from fumaroles it was shown that metals were transported in magmatic vapour, predominantly as chloride species (Symonds *et al.*, 1987). Experimental work by Seward *et al.* (2000) has demonstrated that at 300–350°C, indium is preferably transported by the hydrothermal fluids as chloride ($InCl_4^-$) or hydrolysed ($InClOH^+$) complexes. Fluid inclusion studies of the Sarvlaxviken veins show that metals and quartz precipitated from fluids with low to moderate salinities. Other In-enriched veins are typically characterized by <9 eq. mass% NaCl (Schwarz-Schampera and Herzig, 2002; Seifert and Sandmann, 2006; Sinclair *et al.*, 2006; Jovic *et al.*, 2011; Shimizu and Morishita, 2012; Dill *et al.*, 2013). In the fluid inclusion study of the Mangabeira Sn-In deposit, Moura *et al.* (2014) recorded a large range of salinities, comparable to what now has been documented for the ore-forming fluid in the Sarvlaxviken area, i.e. in the range from 0 to 20 eq. mass% NaCl. Progressive cooling, shown by the spread in temperatures and salinities, has been explained as a result of mixing/dilution of the hot magmatic vapour with cooler meteoric water. The latter is suggested especially for epithermal deposits (Heinrich, 2005; Seifert and Sandmann, 2006). However, an initial single-phase magmatic fluid can separate into coexisting phases with variable vapour to liquid ratios of low-salinity vapour and liquid with a higher salt content in response to declining *P-T* conditions (Heinrich, 2005). As demonstrated in the present study of the ore-forming conditions in the Sarvlaxviken area, the wide variations in temperatures (from 100 to 500°C) and salinities (from 0 to 16 eq. mass% NaCl) can, as an alternative, be the results of combined processes involving condensation, cooling and boiling.

Conclusions

The In-bearing polymetallic quartz veins in the Sarvlaxviken area can be divided into three distinct generations (#1, #2a and #2b) based on their structural relationships and distinct metal associations. The latest metal-bearing vein generation (#2b) has exceptional indium grades (up to 1500 ppm) and shows evidence of brittle fracturing in open spaces. Fluid inclusion evidence presented in this study, provides new information on the transport and depositional processes of metals in anorogenic granites. The study shows that the combined phase separating processes; condensation, cooling and boiling of an aqueous magmatic vapour, enriched in CO_2-F-Cl-S and metals, generated the In-bearing polymetallic veins in the Sarvlaxviken area. The combined processes resulted in a separation of the hot magmatic vapour into a liquid with enhanced salinities (up to 16 eq. mass% NaCl) and a low-salinity (<3 eq. mass% NaCl) vapour. Deposition occurred at temperatures from ~500°C to <100°C in a turbulent flow with complex geometry. Fluid inclusion data show that the depositional conditions were similar regardless of vein generation. The results point towards a model where the accumulation of specific metals at different vein sites or vein generations to a large extent depend on the relative abundance of transporting complexes; chloride in the liquid-dominated phase and sulfur species in the vapour-rich phase.

Even though no fluid inclusion data were generated for the metal-rich alteration veins in the Lillträsket and Marviken areas, it is assumed that the fluids that created these metal accumulations were of the same kind as the fluids that were responsible for the polymetallic quartz veins in the Sarvlaxviken area. All these fluids are considered to have been generated by the F-rich Marviken granite (and dykes), which show all geochemical criteria for an ore-fertile granite.

The investigated quartz veins in the Lillträsket area are considered to represent a very late vein generation (#3), that were deposited from the final residual low-temperature and (at this stage) barren fluid phase.

Acknowledgements

Financial support for this study was received from the K.H. Renlund Foundation. Arto Peltola is thanked for the preparation of doubly polished thin sections. The constructive comments of reviewers (Jens Andersen and Maria Pura Alfonso) contributed to improvement of this manuscript.

References

Audétat, A. and Günther, D. (1999) Mobility and H_2O loss from fluid inclusions in natural quartz crystals. *Contributions to Mineralogy and Petrology*, **137**, 1–14.

Bakker, R.J., Dubessy, J. and Cathelineau, M. (1996) Improvements in clathrate modelling: I. The H_2O-CO_2 system with various salts. *Geochimica et Cosmochimica Acta*, **60**, 1657–1681.

Bodnar, R.J. (2003) Introduction to aqueous-electrolyte fluid inclusions. Pp. 81–99 in: *Fluid Inclusions: Analysis and Interpretation* (I. Samson, A. Anderson and D. Marshall, editors). Mineralogical Association of Canada Short Course Series **32**.

Bodnar, R.J., Burnham, C.W. and Sterner, S.M. (1985) Synthetic fluid inclusions in natural quartz. III. Determination of phase equilibrium properties in the system H_2O-NaCl to 1000°C and 1500 bars. *Geochimica et Cosmochimica Acta*, **49**, 1861–1873.

Cook, N.J., Ciobanu, C.L., Shimizu, M., Danushevskiy, L., Valkama, M. and Sundblad, K.L. (2008) Trace element geochemistry of sphalerite: insights from LA-ICP-MS analysis. *Geologi Lehti, Helsinki*, no. 5, 136–137.

Cook, N.J., Sundblad, K., Valkama, M., Nygård, R., Ciobanu, C.L. and Danyushevsky, L. (2011) Indium mineralization in A-type granites in southeastern Finland: insights into mineralogy and partitioning between coexisting minerals. *Chemical Geology*, **284**, 62–73.

Costi, H.T., Dall'Agnol, R., Pichavant, M. and Rämö, O.T. (2009) The peralkaline tin-mineralized Madeira cryolite albite-rich granite of Pitinga, Amazonian Craton, Brazil: Petrography, mineralogy and crystallization processes. *Canadian Mineralogist*, **47**, 1301–1327.

Davis, D.W., Lowenstein, T.K. and Spencer, R.J. (1990) Melting behaviour of fluid inclusions in laboratory-grown halite crystals in the systems NaCl-H_2O, NaCl-KCl-H_2O, NaCl-$MgCl_2$-H_2O, and NaCl-$CaCl_2$-H_2O. *Geochimica et Cosmochimica Acta*, **54**, 591–601.

Dill, H.G., Garrido, M.M., Melcher, F., Gomez, M.C., Weber, B., Luna, L.I. and Bahr, A. (2013) Sulfidic and non-sulfidic indium mineralization of the epithermal Au-Cu-Zn-Pb-Ag deposit San Roque (Provincia Rio Negro, SE Argentina) – with special reference to the "indium window" in zinc sulphide. *Ore Geology Reviews*, **51**, 103–128.

Gaál, G. and Gorbatschev, R. (1987) An outline of the Precambrian evolution of the Baltic Shield. *Precambrian Research*, **35**, 15–52.

Heinrich, C.A. (2005) The physical and chemical evolution of low-salinity magmatic fluids at the porphyry to epithermal transition: a thermodynamic study. *Mineralium Deposita*, **39**, 864–889.

Heinrich, C.A., Günther, D., Audétat, A., Ulrich, T. and Frischknecht, R. (1999) Metal fractionation between magmatic brine and vapor, determined by microanalysis of fluid inclusions. *Geology*, **27**, 755–758.

Jovic, S.M, Guido, D.M., Schalamuk, I.B., Ríos, F.J., Tassinari, C.C.G. and Recio, C. (2011) Pingüino In-bearing polymetallic vein deposit, Deseado Massif, Patagonia, Argentina: characteristics of mineralization and ore-forming fluids. *Mineralium Deposita*, **46**, 257–271.

Kurhila, M., Mänttäri, I., Vaasjoki, M., Rämö, O.T. and Nironen, M. (2011) U-Pb geochronological constraints of the late Svecofennian leucogranites of southern Finland. *Precambrian Research*, **190**, 1–24.

Moura, M.A., Botelho, N.F., Olivo, G.R., Kyser, K. and Pontes, R.M. (2014) Genesis of the Proterozoic Mangabeira tin-indium mineralization, Central Brazil: Evidence from geology, petrology, fluid inclusion and stable isotope data. *Ore Geology Reviews*, **60**, 36–49.

Nygård, E. (2016) *Geologiska och geokemiska undersökningar av sena rapakivigranit-intrusioner i den sydvästra delen av wiborgbatoliten*. MSc thesis [in Swedish], Åbo Akademi University, Sweden, 62 pp.

Qian, Z., Xinzhi, Z., Jiayong, P. and Shuxun, S. (1998) Geochemical enrichment and mineralization of indium. *Chinese Journal of Geochemistry*, **17**, 221–225.

Rämö, O.T. and Haapala, I. (1995) One hundred years of Rapakivi Granite. *Mineralogy and Petrology*, **52**, 129–185.

Rämö, O.T. and Haapala, I. (2005) Rapakivi granites. Pp 533–562 in: *Precambrian Geology of Finland – Key to the Evolution of the Fennoscandian Shield* (M. Lehtinen, P.A. Nurmi and O.T. Rämö, editors) Elsevier B.V., Amsterdam.

Roedder, E. (editor) (1984) *Fluid inclusions*. Reviews in Mineralogy, **12**. Mineralogical Society of America, Washington, D.C., 644 pp.

Roedder, E. (1992) Fluid inclusion evidence for immiscibility in magmatic differentiation. *Geochimica et Cosmochimica Acta*, **56**, 5–20.

Schwarz-Schampera, U. and Herzig, P.M. (2002) *Indium. Geology, Mineralogy, and Economics*. Springer-Verlag, Berlin Heidelberg.

Seifert, T. and Sandmann, D. (2006) Mineralogy and geochemistry of indium-bearing polymetallic vein-type deposits: Implications for host minerals from the Freiberg district, Eastern Erzgebirge, Germany. *Ore Geology Reviews*, **28**, 1–31.

Seward, T.M., Henderson, C.M.B. and Charnock, J.M. (2000) Indium(III)chloride complexing and sölvation in hydrothermal solutions to 350 : an EXAFS study. *Chemical Geology*, **167**, 117–127.

Shimizu, T. and Morishita, Y. (2012) Petrography, chemistry, and near-infrared microthermometry of indium-bearing sphalerite from the Toyoha polymetallic deposit, Japan. *Economic Geology*, **107**, 723–735.

Simonen, A. and Vorma, A. (1969) Amphibole and biotite from rapakivi. *Geological Survey of Finland*, *Bulletin*, **238**, 28 pp.

Sinclair, W.D., Kooiman, G.J.A., Martin, D.A. and Kjarsgaard, I.M. (2006) Geology, geochemistry and mineralogy of indium resources at Mount Pleasant, New Brunswick, Canada. *Ore Geology Reviews*, **28**, 123–145.

Sun, S. (1982) Chemical composition and origin of the earth´s primitive mantle. *Geochimica et Cosmochimica Acta*, **46**, 179–192.

Symonds, R.B., Rose, W.I., Reed, M.H., Lichte, F.E. and Finnegan, D.L. (1987) Volatilization, transport and sublimation of metallic and non-metallic elements in high temperature gases at Merapi Volcano, Indonesia. *Geochimica et Cosmochimica Acta*, **51**, 2083–2101.

Vaasjoki, M., Rämö, O.T. and Sakko, M. (1991) New U-Pb ages from the Wiborg rapakivi area: constraints on the temporal evolution of the rapakivi granite-anorthosite-diabase dyke association of southeastern Finland. *Precambrian Research*, **51**, 227–243.

Valkama, M., Sundblad, K., Cook, N.J. and Ivashchenko, V.I. (2016*a*) Geochemistry and petrology of the polymetallic skarn ores at Pitkäranta, Ladoga Karelia, Russia. *Mineralium Deposita*, **51**, 823–839.

Valkama, M., Sundblad, K., Nygård, R. and Cook, N.J. (2016*b*) Mineralogy and geochemistry of indium-bearing polymetallic veins in the Sarvlaxviken area, Lovisa, Finland. *Ore Geology Reviews*, **75**, 206–219.

van den Kerkhof, A. and Thiéry, R. (2001) Carbonic inclusions. *Lithos*, **55**, 49–68.

Villar, A. (2017) *Thermal and hydrothermal influence of rapakivi igneous activity on Late-Svecofennian granites in southeastern Finland*. MSc thesis, University of Turku, Finland, 80 pp.

Villar, A., Sundblad, K. and Lokhov, K. (2016). Thermal and hydrothermal influence of rapakivi igneous activity on Late Svecofennian granites in SE Finland. Pp. 114–115 in: *32th Nordic Geol. Winter Meeting, Helsinki*. Bulletin of the Geological Survey of Finland, Special **Vol. 1**.

Vind, J. (2014) *Magnetic susceptibility of crystalline basement and soil, Loviisa area, southern Finland*. MSc thesis, University of Tartu, Estonia, 41 pp.

Vorma, A. (1972) On the contact aureole of the Wiborg rapakivi massif in southern Finland. *Geological Survey of Finland*, *Bulletin*, **255**, 28 pp.

Wilkinson, J.J. (2001) Fluid inclusions in hydrothermal ore deposits. *Lithos*, **55**, 229–272.